11. Supplementary Information

11.1. Single particle motion

Here, we show that the update of the orientation vector $\mathbf{e_i}(t)$ based on the laser position $\mathbf{l_i}(t)$, i.e. $\boldsymbol{e}_i(t) = (\boldsymbol{r}_i(t) - \mathbf{l_i}(t))/|\boldsymbol{r}_i(t) - \mathbf{l_i}(t)|$, gives the right dynamics for the single particle motion. In Fig. S1, we compare single-particle motion in simulation and experiment via the angular-velocity auto-correlation $G(t) = \langle\dot{\theta}(t)\dot{\theta}(0)\rangle/\langle\dot{\theta}(0)^2\rangle$, which gives a good agreement and thereby validates the implementation of the update scheme in the simulation.

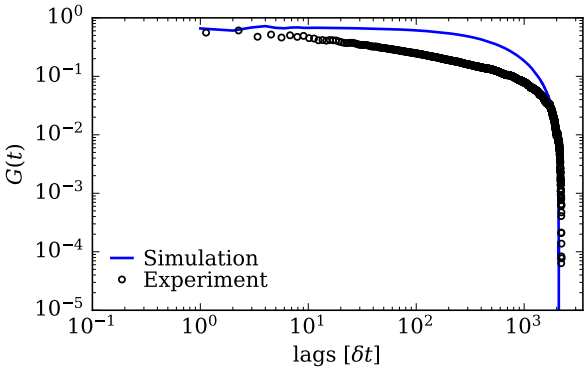

Fig. S1: Single particle dynamics Particle angular velocity auto-correlation in simulations and experiments show very good agreement when the simulation uses the same update scheme (for the laser) as is in the experiment. Here, in both simulation and experiment, passive diffusion coefficient $D_t \simeq 0.03\mu\text{m/s}^2$,$\delta t = 0.4$s and particle speed $u_0 = 2.5\mu$m/s.

11.2. Probing two-particle interactions

To develop the simulation model, a series of additional experiments were performed to determine the simulation parameters which best match the experimental system. Here, an active particle and a passive particle were placed at a initial separation of $\sim$ 30 µm and then the active particle was driven in the direction of the passive particle. This was repeated for different active particle velocities, and the velocity of the passive particle was measured to probe the strength of the hydrodynamic interactions between the particles. This experiment was then replicated in simulations using identical initial conditions. It was observed that a model with only squirmer interactions significantly underestimates the hydrodynamic forces, as shown in Fig. S2 (black lines) due to the fast decay of the (far-field) hydrodynamic forces $\sim r^{-3}$. To address this issue, lubrication forces were incorporated into the simulation model. The lubrication force added described by the flow field

$$\mathbf{U}_{lub,j}(r) = -\frac{a}{h}(\dot{\mathbf{r}}\cdot\hat{\mathbf{r}})\Theta(r)\hat{\mathbf{r}} \tag{15}$$

where $\dot{\boldsymbol{r}} = \dot{\boldsymbol{r}}_i - \dot{\boldsymbol{r}}_j$ is the relative velocity between particle j and i, $h = r - 2a$ is the shortest distance between the surface of the two particles. A cutoff function of the form $\Theta(r) = \exp(-r/R_0)$ captures the finite range of the force, where different the parameter R_0 is varied to match the simulation to the experimental data. For the two-particle experiment, we find that a value $R_0 \simeq 2.0a$ matches the experimentally observed long decay of the hydrodynamic forces (blue lines Fig. S2). However, the grid experiments (see Fig. 1 of main text), suggest a much slower decay of the hydrodynamic forces. Thus, we ultimately selected a value of $R_0 \sim 3.5a$ (Fig. S2 green lines) to achieve reasonable agreement between the simulation data for both the two-particle interaction and the grid experiments. Given the simplicity of the model, our goal is primarily a qualitative agreement with experimental observations, as a quantitative match is challenging at this level of description.

11.3. Synchronization domains

The synchronization of the oscillators at short distances is primarily governed by the (near-field) lubrication force. To study this behavior, we consider a simplified model involving two nearly-synchronized swarmalators rotating around fixed reference positions. We assume that the reference points are fixed at $\boldsymbol{q}_1 = (0, 0)$ and $\boldsymbol{q}_2 = (R_0, 0)$, with the two swarmalators performing a circular trajectory around their

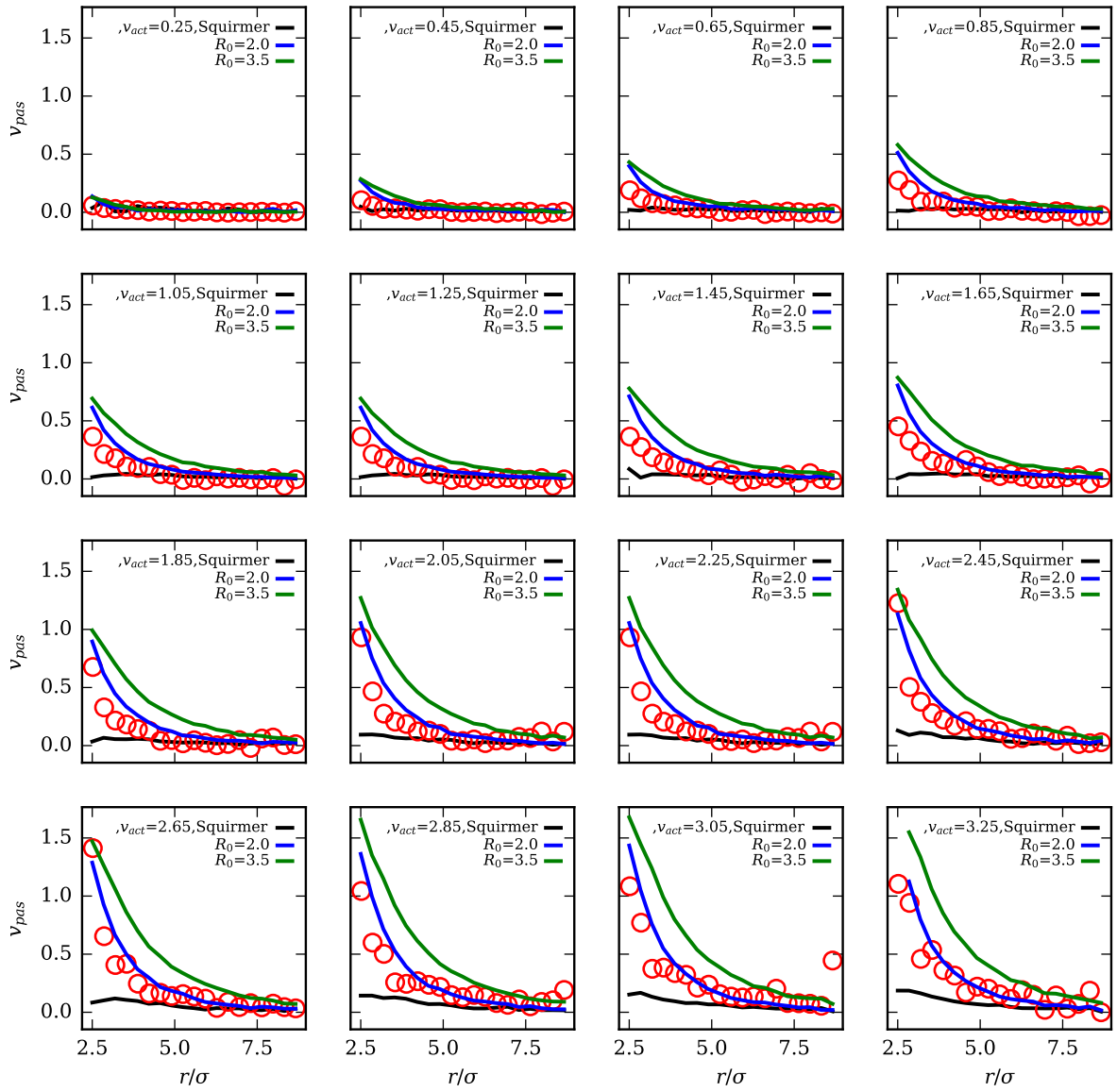

Fig. S2: Binary interactions between an active particle and a passive particle. Velocity v_{pas} of the passive particle as a function of the separation r from the active particle. The different sub-figures correspond to different velocities of the driven particle. Experimental data is shown with red circles, results from the simulation data by solid lines, with different choices of the decay range R_0 (in units of particle radius a).

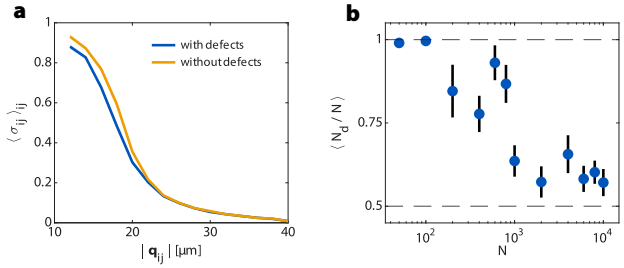

Fig. S3: Synchronization organizes in domains. **a**, Mean synchronization vs the distance of reference positions $|\boldsymbol{q}_{ij}|$ on a grid with defects (blue, as in Fig. 1g in the main text) and without defects (orange). **b**, The mean synchronization domain size normalized by the the system size $\langle N_D/N \rangle$ over the total number of particles in the system N.

respective reference points. The orientation vectors are then given by $\mathbf{e}_1 = \text{sign}(\omega)(\cos\omega t, \sin\omega t)$ and $\mathbf{e}_2 = \text{sign}(\omega)(\cos(\omega t + \epsilon), \sin(\omega t + \epsilon))$, where ϵ is the phase difference between the two swarmalators, and their position vectors by $\mathbf{r}_1(t) = r_0(\sin\omega t, -\cos\omega t)$ and $\mathbf{r}_2(t) = (R_0 + r_0\sin(\omega t + \epsilon), -r_0\cos(\omega t + \epsilon))$, where $r_0 = u_0\omega^{-1}$. The force on particle 2 due to the motion of particle 1 is

$$\gamma^{-1}\mathbf{F}_{2\to1} = \mathbf{U}_{lub,1}(r) \simeq -\frac{au_0}{hR_0^2}[(\mathbf{e}_2 - \mathbf{e}_1)\cdot(\mathbf{r}_2 - \mathbf{r}_1)](\mathbf{r}_2 - \mathbf{r}_1), \tag{16}$$

where we have assumed $|\mathbf{r}_2 - \mathbf{r}_1| \simeq R_0$ and $\Theta(r) \simeq 1$. Then, for $\epsilon \ll 1$, the leading order contribution is obtained as

$$\gamma^{-1}\mathbf{F}_{2\to1}(\epsilon) \simeq -\epsilon\frac{a}{h}u_0\ \text{sign}(\omega)\ \sin(\omega t)\ \hat{\mathbf{x}}. \tag{17}$$

The force at any time thus acts like a spring force, driving the system toward full synchronization, i.e. toward $\epsilon = 0$. A similar calculation can be performed for the (far-field) squirmer interactions, which also yields a spring-like leading-order term from the source dipole. Thus, the long-range synchronization is driven by the squirmer source dipole that decays as $1/r^3$, in agreement with experiments (see equation (3) in the main text).

Figure S3a shows the mean synchronization $\langle\sigma_{ij}\rangle$ against the distance between reference positions $|\boldsymbol{q}_{ij}|$ without defects in comparison to the data from Fig. 1g in the main text, which was computed from systems with defects. The inclusion of defects yields a slightly lower synchronization for small reference point distances. The lower synchronization at shorter distances observed in experiments can therefore be understood as arising from the presence of defects, such as unresponsive or missing particles, whereas the simulation model operates under ideal conditions, leading to higher synchronization.

As mentioned in section 2 in the main text, the oscillators form domains of high synchronization when their reference points are arranged on a grid. We analyzed the domain sizes for different system sizes (without defects) with up to 10,000 oscillators in simulations. The synchronization domains were identified by a synchronization threshold of $\sigma_t = 0.85$ and a clustering analysis on the resulting data. This isolates the synchronized regions via domain walls of lower synchronization. Synchronization is found to be highly robust, with domain size scaling approximately linearly with system size (see Fig. S3b). In particular, for systems with up to 100 particles, complete synchronization is observed, whereas for $N > 1000$, the domain size scales approximately as $N_{domain} \simeq 0.5N$. In the intermediate range, $100 < N < 1000$, the system occasionally achieves full synchronization, but may also form smaller synchronized domains. Since the experimental setup lies within this range, large synchronized regions ($N_{\text{domain}} \propto N$) are likely to emerge; however, the presence of unresponsive particles makes the formation of a fully synchronized cluster unlikely.

11.4. Squirmer Parameter β

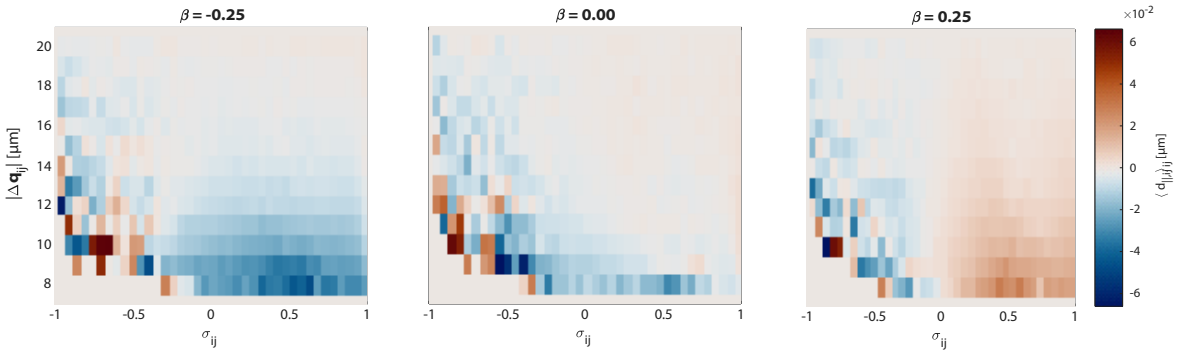

Fig. S4: Heat map of the mean parallel displacement $d_{\parallel,ij}$ for different synchronizations and distance of Delaunay neighbors in simulations, for squirmer parameter $\beta = [-0.25, 0.0, 0.25]$. For $\beta \leq 0$ (pusher), there is no region of net attraction, i.e. the swarmalators are always repelled.

To understand the influence of hydrodynamic forces and synchronization on the overall motion of the particle around the reference point, we analyze the average displacement of the average particle position around the reference position as a function of synchronization and the neighbour distance, as shown in Fig. 4 of the main text. Here for each particle, we compute the displacement and synchronization

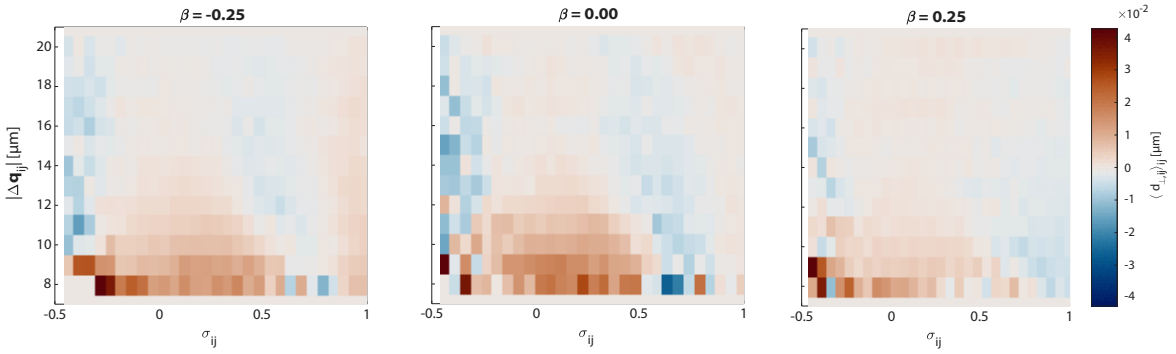

Fig. S5: Heat map of the mean perpendicular displacement $d_{\perp,ij}$ for different synchronizations and distance of Delaunay neighbors in simulations, for squirmer parameter $\beta = [-0.25, 0.0, 0.25]$. For $\beta > 0$ (puller), the data is shows qualitative agreement with the experimental data (Fig. 5f in main text).

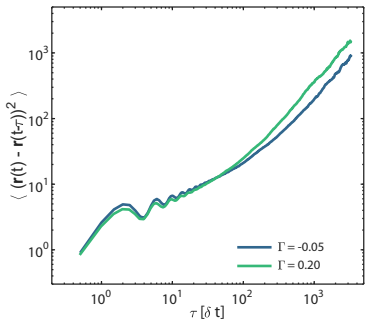

Fig. S6: Mean squared displacement (MSD) of the swarmalators at high density for $\Gamma = 0.2$ and $\Gamma = -0.05$.

averaged over 10 frames, and $\Gamma = 0$, so that the reference positions are fixed. Experimental data show that a pair of swarmalators is attracted when their average synchronization is zero, whereas increasing synchronization causes them to repel each other, resulting in synchronization-dependent pair coupling.

When this analysis is performed in simulations with $\beta = 0$, we do not observe any repulsive regime for the swarmalator pair; the pair is always (weakly) attracted for all values of synchronization, as shown in Fig. S4. To explore the possibility of a non-zero β, we perform simulations for $\beta \in (-1, 1)$. Fig. S4 shows that for pushers, with $\beta < 0$, the swarmalator pair remains attracted across all synchronization values. However, for pullers, with $\beta > 0$, a region of 'repulsive' coupling emerges at higher synchronization, consistent with the experimental observations.

This indicates that swarmalator interactions are highly sensitive to the hydrodynamic flow field — such that even a small change in β can have a non-trivial impact on the collective behavior of the swarmalators. Since the flow field of the light-driven colloids used in the experiment is expected to be similar to that of a neutral squirmer, we choose a small value of $\beta = 0.25$ to qualitatively reproduce the observed behavior. Note that a small positive squirmer parameter is consistent with the presence of a demixing bubble beneath the particle, which moves along with the ABP [30]. This generates an asymmetric flow field, with some qualitative resemblance to a (weak) puller.

To investigate the effect of hydrodynamic interactions on the motion of neighboring swarmalators — and, consequently, on the motility of the reference points — we consider a simplified model involving two fully synchronized swarmalators rotating around fixed reference positions. We assume that the reference points are fixed at $\boldsymbol{q}_1 = (0, 0)$ and $\boldsymbol{q}_2 = (R_0, 0)$, with the two swarmalators performing a circular trajectory around their respective reference points. With this, the orientation vectors are given by $\mathbf{e}_1 = \mathbf{e}_2 = \text{sign}(\omega)(\cos\omega t, \sin\omega t)$, and the difference vector $\hat{\mathbf{r}}(t) = \mathbf{r}_2(t) - \mathbf{r}_1(t) = \hat{x}$. The force on particle 2 due to particle 1 is then given by

$$\gamma^{-1}\mathbf{F}_{2\to1} = \mathbf{U}_{flow,2}(r) = -\frac{p}{r^2}[1 - 3(\mathbf{e}_j \cdot \hat{\mathbf{r}})^2]\hat{\mathbf{r}} - \frac{s}{r^3}[\mathbf{e} - 3(\mathbf{e}_j \cdot \hat{\mathbf{r}})\hat{\mathbf{r}}], \tag{18}$$

where $\mathbf{U}_{lub,2}(r) = 0$ is assumed as they are fully synchronized. This then gives the time dependent force

$$\begin{aligned}\gamma^{-1}\mathbf{F}_{2\to1} = &-\frac{p}{r^2}\left[1 - 3\cos^2\omega t\right]\hat{x} \\ &- \frac{s(\text{sign}(\omega))}{r^3}\left[\cos\omega t\hat{x} + \sin\omega t\hat{y} - 3\cos\omega t\hat{x}\right]\end{aligned} \tag{19}$$

Averaging this force over one cycle of rotation results in

$$\gamma^{-1}\mathbf{F}_{2\to1} = \frac{p}{2r^2}\hat{x} = -\gamma^{-1}\mathbf{F}_{1\to2} \tag{20}$$

This implies that for $p = 0$ (neutral squirmer), there is no net interaction between the rotating particles, i.e., $p \neq 0$ is necessary for the swarmalators to interact with each other (in the fully synchronized state). In particular, we find that for $p < 0$, i.e., $\beta > 0$ (puller), the swarmalator pair is attracted towards each other, thus rationalizing the experimental results observed and our choice of β in the simulation.

Simulation data for $\langle d_{\perp,ij}\rangle_{ij}$ shows that the lateral force also depends on β, with $\beta > 0$ and $\beta < 0$ resulting in opposite values for the perpendicular force component (Fig. S5). Again, the data for $\beta > 0$ shows a qualitative match with the experimental data. We can qualitatively understand this by assuming in our previous 'toy' model of two perfectly synchronized particles on circular trajectories, the center of rotation of the second particle is slightly displaced from the reference position. This implies that it performs a rotation around the point (R_0, ϵ), which would then give us a force

$$\gamma^{-1}\mathbf{F}_{2\to1} = \frac{p}{2r^2}\frac{\hat{x} + \epsilon\hat{y}}{1 + \epsilon^2} = -\gamma^{-1}\mathbf{F}_{1\to2}, \tag{21}$$

i.e., the perpendicular force (projected onto $\hat{y}$ – the connection vector perpendicular to $\boldsymbol{q}_1 - \boldsymbol{q}_2$) depends on the squirmer parameter p, thus rationalizing the data seen for $\langle s\rangle \simeq 1$ in Fig. S5. However, note that this simple model does not clarify where the angular velocity comes into play or how the perpendicular force is sustained (i.e., why it doesn't average out to zero).

11.5. Swarmalator motility in switching experiments

In the experiment that produced a state loop (see Fig. 5 in the main text), we switched Γ between 0.2 and -0.05. We selected these two values of Γ because they result in the same swarmalator motility and therefore let the Γ-switch only affect the attraction / repulsion behavior. Fig. S6 shows the MSDs of swarmalators at the same density as used in the state-loop experiments for these two values of Γ.

11.6. Supplementary Videos

- Supplementary video 1: **Hydrodynamic synchronization on a grid.** Shows the oscillation of ABPs around reference positions arranged on a hexagonal grid for a lattice spacing of $D = 12, 18$ and 24µm in experiment and simulation. The ABPs are color coded according to their synchronization σ_i to their neighbors.

- Supplementary video 2: **Interacting swarmalators with negative and positive Γ.** Time evolution of exemplary runs during the first 8000 δt of dense systems of swarmalators for $\Gamma = -0.1$ and $\Gamma = 0.2$ in experiment and simulation (as in Fig. 3 in the main text). Swarmalators are colored according to their synchronization σ_i to their neighbors.

- Supplementary video 3: **Animated phase diagram of the swarmalator model.** Shows the time evolution of dense swarmalator systems from numerical simulations of the swarmalator model given in equation (3) and equation (4) in the main text for the same values of K and J Fig. 4. The swarmalators are colored according to their phase.